Molecular mobility and relaxation process of isolated lignin studied by multifrequency calorimetric experiments

Nathanael Guigo, Alice Mija,* Luc Vincent and Nicolas Sbirrazzuoli

Received 21st July 2008, Accepted 4th November 2008
First published as an Advance Article on the web 7th January 2009
DOI: 10.1039/b812512k

The glass transition of lignin has been studied by multifrequency calorimetric measurements in order to highlight the morphological changes and the dynamic aspects associated to this relaxation process. Influences of water sorption and thermal annealing on molecular mobility have been considered. Additional investigations by thermogravimetry, infra-red spectroscopy and rheometry have been performed to corroborate the claims. The relaxation process of annealed lignin shows a different behaviour as the consequence of micro-structural modifications of lignin. These are explained by redistribution of secondary bonds as well as formation of new interunit linkages. Concerning the dynamic aspects, apparent activation energy, E, and sizes of cooperatively rearranging region, V_{crr}, have been evaluated respectively from the frequency dependence and heat capacity measurements of the glass transition. Compared to dried lignin, both E and V_{crr} significantly decrease in a water-sorbed matrix indicating that the three-dimensional structure presents a higher mobility and is less confined.

Introduction

Native lignin is a three dimensional amorphous polymer of high molecular weight which interbinds the cellulosic micro-fibrils. Its thermal softening is mainly responsible for the viscoelastic properties of wood.[1–3] In the papermaking industry, most of the lignin is used as fuel and only small amounts (1–2%) are isolated at the industrial scale.[4] The sources of isolated lignin can be classified into Kraft lignin, lignosulfonate and sulfur-free lignin. The latter class is obtained from the organosolv and soda pulping process as well as biomass conversion processes.[5] Isolated lignins differ from their native biomacromolecules in terms of chemical structure and physical properties. Such differences are attributed to the delignification process, which induce partial depolymerization of the native lignin by cleavage of α- or β-aryl ether bonds.[6]

For many years, lignin has been blended with various thermoplastic matrix such as polypropylene (PP),[7–9] polyethylene (PE),[7,10] polystyrene (PS),[7,10,11] polyethylene oxide (PEO),[7,12,13] polyvinylchloride (PVC)[14–16] and many more.[17–21] In certain cases, addition of this natural polymer has improved anti-oxidant[8] or antifungal[14] properties of the end-products. A perfect knowledge of lignin thermal behaviour is challenging in order to determine the optimum parameters for compounding this complex macromolecule. Isolated lignins are completely amorphous and undergo a thermal softening. Since the first investigations of Goring,[22] different studies have been devoted to the thermal behaviour of isolated lignin. A great contribution to elucidate this aspect has been done by Hatakeyama *et al.*,[23–28] nevertheless the difference between thermal softening and thermo-mechanical relaxation (associated with the mechanical manifestation of the glass transition) remains unclear. Dynamic mechanical analysis (DMA)[29] or infra-red spectroscopy[24,30] have been used, but differential scanning calorimetry (DSC)[25–28,31–33] remains the most employed technique. According to these studies, the glass transition temperature (T_g) of isolated lignins, which usually ranges between 80 °C and 200 °C, is influenced by molecular weight,[27,32] delignification processes,[32] and thermal histories[25,33] or origins[31] (*i.e.* softwood, hardwood or annual crops lignins). These high T_g values are linked to the low mobility of lignin chains which are mainly constituted by rigid aromatic units. Due to the presence of polar groups, hydrogen bonds have a significant contribution to the molecular mobility of lignin segments.[30,34] Moreover, as in the case of soils, sediment and other natural sorbants, the large disparity in macromolecular mobility of lignin chains can result in widely varying sorption behaviour. When water is sorbed on specific sites, it acts as an efficient plasticizer especially for low water content[28,35,36] ($<5\%$).

As the endothermic volatilization of sorbed water hides the sigmoidal variation of heat capacity (C_p) during glass transition, most of the conventional DSC studies report T_g values measured on dried lignin (*i.e.* during the second DSC run after previous volatilization of water). This approach, however, has inevitably certain drawbacks since the measured T_g value at the second run does not exactly reflect the initial state of the material because during the drying cycle, morphological changes occur on lignin. For this reason, temperature modulated DSC (TMDSC),[37] that enables one to separate reversing and non-reversing thermal events, gives new insights in the study of glass transition of synthetic polymers and can be advantageous to explore the complex thermal behaviour of natural polymers. Recently, a new multifrequency TMDSC technique, TOPEM®, has been developed by Schawe *et al.*[38]

Thermokinetic Group, Laboratory of Chemistry of Organic and Metallic Materials C.M.O.M., Institute of Chemistry of Nice (CNRS FR3037), University of Nice—Sophia Antipolis, 06108 Nice Cedex 2, France. E-mail: mija@unice.fr

from Mettler-Toledo and has been applied to the glass transition of polycarbonates,[39] polystyrene[40,41] and maltitol.[42] Compared to TMDSC which imposes a sinusoidal modulation of heating rate, TOPEM® uses a stochastic modulation of temperature. This technique allows the evaluation of the "quasi-static" heat capacity (C_{p0}) and the separation of the total heat flow in two components, the reversing (Φ_{rev}) and non-reversing heat flows ($\Phi_{non\text{-}rev}$). The major advantage of TOPEM® over TMDSC is the determination in one single experiment of the complex heat capacity for a wide range of frequencies using just one sample. This latest ability is particularly interesting to study the kinetics of frequency-dependent phenomena such as the cooperatively α-process involved in the mechanical manifestation of the glass transition. The dynamic glass transition temperature (T_α) corresponding to the α-relaxation is usually measured by dynamic mechanical and dielectric techniques. In TMDSC, the dynamic T_α is evaluated from the heat capacity signal which is frequency dependent and has been distinguished[43–46] from the so-called thermal T_g which depends on the underlying heating (cooling) rate. Kinetic studies of the glass transition are usually based on the Tool[47]–Narayanaswamy[48]–Moynihan[49] (TNM) model where a single value of apparent activation energy (E) can be determined from the dependence of T_α on frequencies. In previous TMDSC studies, these dependences have been fitted by a linear Arrhenius[46,50] or non-linear Vogel–Tammann–Fulcher (VTF) equations.[51–53] A modified Narayanaswamy model has been proposed by Kahle *et al.*[54] in order to determine point by point the underlying equilibrium time of T_α in certain frequencies regions. The constancy of the apparent activation energy throughout the glass transition of various polymers has been recently questioned by Vyazovkin *et al.*[55] who have obtained a decreasing of E values with extent of conversion using an advanced isoconversional method applied to DSC data. These authors demonstrate that the decrease of E values can be interpreted in term of a decrease in the degree of cooperativity throughout the glass transition. The rate of this variation has been correlated with the dynamic fragility of the glass forming systems.[56]

Concerning the glass transition of lignins, two cases must be considered. For *in situ* lignin, the glass transition kinetics has been evaluated from DMA[1,57,58] or differential thermal analysis (DTA)[59] measurements made on wood samples. According to these studies, the temperature dependence of relaxation times follows a Williams–Landel–Ferry (WLF) equation. On the contrary, the glass transition kinetics of isolated lignins has never been studied yet, probably because for such powdered materials this transition has been considered more as a rubbery softening instead of a true α-relaxation.[59]

In the present study, the glass transition of isolated lignin is evaluated by multifrequency temperature modulated DSC. To our knowledge, this is the first time that the glass transition of lignin has been analysed by a temperature modulated DSC technique. Influence of sorbed water on the relaxation processes has been considered and then, experiments in open and sealed crucibles have been conducted. The former type of crucibles allows dehydration of sorbed water during heating, whereas for the latter the water stays in the media and its effect on the molecular mobility can be analyzed. The importance of thermal annealing on the glass transition behaviour is also discussed in this paper. Comparisons between first run (without previous thermal treatment) and second run (after an annealing cycle) measurements have been made. Additional FTIR spectroscopy, thermogravimetric and rheometric measurements have been performed to confirm the importance of molecular interactions between water and lignin chains and to highlight the role of cooperatively segment relaxations. Finally, from the multifrequency curves of the complex heat capacity, the apparent activation energies (E) of glass transition and the size of cooperatively rearranging region (V_{crr}) of dehydrated and water-sorbed lignins are evaluated.

Experimental

Materials

The Alcell lignin (AL lignin) was obtained from Repap Technologies Inc., Valley Forge, PA, USA. It was obtained from a mix of hardwoods, approximately 50% maple, 35% birch and 15% poplar, and was isolated by an ethanol-based organosolv pulping process. The organosolv process is an autocatalysed acid process in which the organic solvent promotes impregnation in plant tissues. Hydrolysis of acetyl groups present on hemicellulose generates acetic acid that allows delignification and partial hemicellulose hydrolysis.[60,61] Hardwood Alcell lignin has already been used as lignin reference in previous studies.[62,63]

The lignin powder was passed through a sieve (200 μm) prior to use. The molecular weight of AL lignin has been determined at University of Wageningen by size exclusion chromatography (SEC) in DMF. Its polydispersity is about $\sim$5.21 ($M_n \sim 536$ and $M_w \sim 2794$ g mol^{-1}). Its reported T_g value is $\sim$97 °C and the solid powder density is $\sim$1.27 g cm^{-3}. More details on AL lignin analytical data can be found elsewhere.[60,64]

Experimental techniques

DSC measurements were made on a Mettler-Toledo DSC 823^e and STAR© software for data analysis. The apparatus is equipped with a HSS7 ceramic sensor (heat-flux sensor with 120 thermocouples Au–Au/Pd), which allows very high sensitivity. Temperature and enthalpy calibrations were performed by using indium and zinc standards. Integrations of DSC peaks were done using a linear baseline. Wet AL lignin samples ($\sim$15 mg) were placed in "open crucibles" (40 μL aluminium crucibles with one small pinhole punctured on the top) or in "sealed crucibles" (high pressure 30 μL stainless steel crucibles) in order to highlight the influence of sorbed water on the glass transition. The former allows volatilization of water during the heating as for the latter, the water remains into the lignin sample. All the pans were sealed under nitrogen.

The measurements were conducted at an underlying heating rate of 1 K min^{-1} with a scanning temperature ranging from 20 °C to 220 °C. The amplitude was fixed at ±0.5 K for all the modulated experiments. The period of pulses were ranging from 30 to 60s for the experiments conducted in open crucibles. As the τ lag of the sealed crucibles is higher, the time between pulses ranged from 90 s to 240 s. In the

TOPEM® mode, no correction of the heat flow by an empty run is needed, since the mass of both reference and sample crucibles are entered into the method.

The glass transition of amorphous polymers, such as lignin, is closely linked to their thermal histories.[25] Two multi-frequency DSC scans were conducted. The first scan was without any thermal treatment and at the second scan was after a temperature program to remove the thermal history of the sample. During this thermal treatment, the samples were heated in DSC from 25 °C to 135 °C, held at this temperature for 30 min and cooled down to 20 °C at a rate whose absolute value is equal to the TOPEM® underlying heating rate (*i.e.* 1 K min^{-1}). The evaluations were made on the heat flow response to the stochastic modulation of temperature. The calculation window width was fixed to 600 s and smoothing window to 450 s. For the experiments conducted with open crucibles, frequencies (*f*) of 4, 8, 16, 24 and 32 mHz have been selected. In sealed crucibles, the τ lag is significantly higher and consequently, lower frequencies have been selected of 1.28, 1.92, 2.56 and 3.20 mHz.

FTIR analysis of water-sorbed and annealed lignin samples were performed on a Perkin Elmer Spectrum BX II spectrophotometer. The annealed lignin was submitted to the same temperature program used to remove thermal history in DSC (heating to 135 °C and cooling to 20 °C under nitrogen atmosphere). To increase the signal to noise ratio, a total of 128 scans were accumulated for each measurement, at a spectral resolution of 4.0 cm^{-1}. The spectra were collected as KBr pellets at an accurate lignin concentration of 1 wt%. The recorded spectra were baseline corrected and correspond to the mean spectra of three measurements.

Thermogravimetric analysis (TGA) was used to estimate the water content and the onset of thermal decomposition of the AL lignin. These experiments were conducted on Mettler-Toledo TGA 851^e between 20 °C to 300 °C at a heating rate of 1 K min^{-1} under a nitrogen flow of 50 mL min^{-1}. The TGA microbalance has a precision of ±0.1 μg.

Rheometric measurements were conducted on oscillating mode with parallel plate geometries (15 mm diameter and 1 mm gap, striated plates) of a Bohlin C-VOR rheomether with strain convection heating. Measurements were carried out on auto stress mode with a frequency of 1 Hz, and a deformation of 0.05%. The rheometric measurements were conducted at heating rate of 1 K min^{-1} with a scanning temperature ranging from 30 °C to 250 °C. First and second DSC scans were also considered. The second DSC scan was made immediately after the above mentioned annealing cycle to 135 °C. As the lignin is a powdered solid, it was pressed at 5 tons in a specially designed mould before performing the rheometric experiments. The pressed lignin sample forms a solid pellet between the striated plates. Due to this sample state the measured modulii does not correspond to those obtained as in the case of massive samples. It should be also mentioned that friction between individual particles in pressed powders can lead to dissipative contributions and accordingly the measured modulii are considered as apparent values.

All mentioned experiments have been conducted at least three times to ensure that observed phenomena were not artefacts.

Size of cooperatively rearranging region (V_{crr})

The size of cooperatively rearranging region (V_{crr}) derived from the molecular–kinetic theory of Adam and Gibbs[65] gives a spatial aspect of dynamic heterogeneity. The evaluation of heat capacity curves data gives the essential parameters to calculate the V_{crr}. Its value is determined from the thermodynamic fluctuation formula of Donth:[66,67]

$$V_{crr} = \frac{k_B T_g^2 \Delta(C_v^{-1})}{\rho(\delta T)^2} \quad (1)$$

where k_B is the Boltzman constant, T_g is the glass transition measured at the midpoint of sigmoidal C_{p0} variation and ρ the density. C_v represents the isochoric heat capacity. A correction factor, S, relates $\Delta(C_v)$ with $\Delta(C_p)$.

$$S \equiv \frac{\Delta(C_v^{-1})}{\Delta(C_p^{-1})} = 0.74 \pm 0.22 \quad (2)$$

The mean square temperature fluctuation, $(\delta T)^2$ can be estimated from the Gauss fit of imaginary part of heat capacity (C''_p):

$$C''_p(T) = \text{const} \times \exp(-(T - T_\omega)/2\delta T^2) \quad (3)$$

where δT represents the dispersion of the Gauss transformation and T_ω is the maximum peak temperature of the C''_p curve.[67]

Results and discussion

Dehydration of lignin during glass transition (open crucible experiments)

Fig. 1 represents the measured heat flow of wet AL lignin in response to the stochastic pulse of temperature. This multi-frequency DSC experiment was conducted in open crucibles during the first run. The total heat flow curve that is derived from the measured heat flow is represented in the same graph by a solid line. This curve corresponds to the same heat flow

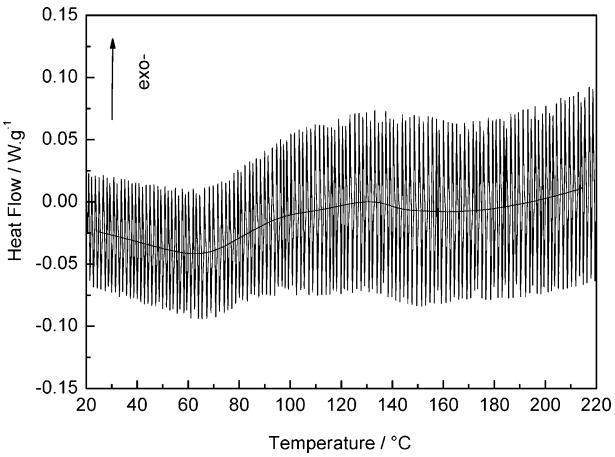

Fig. 1 Measured heat flow in response to the series of stochastic temperature pulses. The measurement on water-sorbed AL lignin was registered during the first scan in open crucibles. The total heat flow curve derived from the measured heat flow after TOPEM® evaluation is represented on the graph by a solid line.

response that would be obtained by conventional DSC. As the lignin sample had not been previously dried, dehydration was predominant and hid other thermal events that occur in the same temperature range. According to this curve, no glass transition can be highlighted. However, by analyzing the correlation between the measured heat flow and the instantaneous heating rate, the TOPEM® method permits separation of the total heat flow into the reversing and non-reversing heat-flow components.

Fig. 2 shows the reversing (Φ_{rev}) and non-reversing ($\Phi_{non\text{-}rev}$) heat flows obtained after mathematical treatment of the measured heat flow. According to the adopted convention a decrease in the heat flux curve (exothermic is up in the Figures) corresponds to an increase in the heat capacity. The first and second DSC scans are shown in the same graph. As illustrated in Fig. 2, the characteristic sigmoidal variation of the Φ_{rev} curve can be unequivocally attributed to the glass transition of AL lignin and this transition is separated from non-reversible thermal events. Table 1 gathers the midpoint temperature (T_{mid}), the glass transition interval ($\Delta T_{set} = T_{endset} - T_{onset}$) and the difference in heat capacity between glassy and rubbery states, $\Delta(C_{p0})$.

In preceding conventional DSC studies,[23,33,35] the glass transition of lignin was obtained only during the second run, after a drying cycle. In the present work, the glass transition of lignin can be directly evaluated from the reversing TOPEM® heat flow during the first heating scan (*i.e.* during the dehydration process). According to Fig. 2, this transition shows clear differences compared to the transition measured during the second scan. First, as seen from Table 1 in the open crucible column, $(\Delta C_{p0})_{1st\ run}$ is lower than $(\Delta C_{p0})_{2nd\ run}$. As vaporization of sorbed water occurs during the first scan, the increase in heat capacity at the glass transition is partly compensated by its decrease due to dehydration. Then, the difference in $\Delta(C_{p0})$ between the first and second runs, $(\Delta C_{p0})_{2nd\ run} - (\Delta C_{p0})_{1st\ run} \sim 0.12$ J g^{-1} K^{-1}, corresponds to the water vaporized during the first run. Considering the heat capacity of water (4.179 J g^{-1} K^{-1}) the amount of sorbed water can be calculated at ~2.9% w/w. It can be also noted

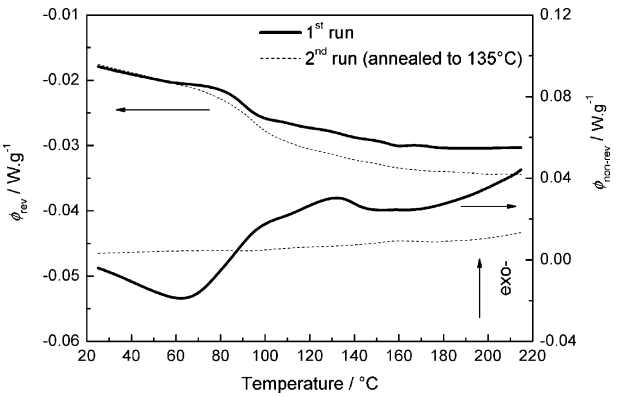

Fig. 2 Reversing (Φ_{rev}) and non-reversing ($\Phi_{non\text{-}rev}$) heat flow derived from the total heat flow response to stochastic temperature pulses obtained during the heating of water-sorbed AL lignin in open crucibles. The measurements were registered during the first run (solid line) and during the second run (dash line) after an annealing cycle to 135 °C.

Table 1 Mid-point temperature (T_{mid}), glass transition interval (ΔT_{set}) and difference in heat capacity (ΔC_{p0}) corresponding to the glass transition of AL lignin in various experimental conditions

	Open crucibles		Sealed crucibles		
TOPEM® mode 1 K min^{-1}	1st run	2nd run (after annealing to 135 °C)	1st run T_{g1}	1st run T_{g2}	2nd run (after annealing to 135 °C)
T_{mid}/°C	89.6	92.6	59.6	92.9	60.3
ΔT_{set}/°C	16.7	23.7	16.6	19.0	33.5
ΔC_{p0}/J g^{-1} K^{-1}	0.31	0.43	0.42	0.15	0.51

that the $(\Delta C_{p0})_{2nd\ run}$ (Table 1) is in good agreement with previous works of Hatakayema *et al.*[26] ($\Delta C_p \sim 0.50$ J g^{-1} K^{-1}) and Leboeuf *et al.*[33] ($\Delta C_p \sim 0.45$ J g^{-1} K^{-1}) conducted by regular DSC on dried lignin. The glass transition temperature T_{mid} obtained after the second run (Table 1, open crucible column) is shifted to higher temperature (~3 °C) and ΔT_{set} significantly increases. During the first run, the plasticizing effect of water on T_g is very limited because vaporization occurs in the same temperature interval. Then, to explain differences between first and second run, non-reversible thermal events must be considered.

The non-reversing heat flow can generally be associated with the processes that are irreversible on the time scale of the temperature perturbations (typically from seconds to minutes). These irreversible phenomena are shown in Fig. 2, on the $\Phi_{non\text{-}rev}$ curves (bottom curves). When measured at the 1st run, the endothermic peak observed between 20 °C and 100 °C corresponds to vaporization of sorbed water. The heat of vaporization found from integration of this peak is about (63 ± 2) J g^{-1}. Relative to the heat of vaporization of bulk water (2256.8 J g^{-1}), the water content can be estimated at ~ (2.8 ± 0.1) w/w that compares well with the precedent value (2.9%) calculated above. During the second run, no water vaporization is detected suggesting that the previous thermal treatment has completely dried the sample. This is confirmed by TGA experiments conducted in similar conditions to the DSC experiments.

For 100 °C < T < 150 °C an exothermic peak (reaction heat $Q \sim 13 \pm 3$ J g^{-1}) is observable on $\Phi_{non\text{-}rev}$ curve measured during the first run (Fig. 2) and corresponds to irreversible processes that occur above the glass transition. It is well known that in the glassy state, the molecules are frozen in non-equilibrium conformations. When devitrification occurs, further reactions can be reactivated at higher temperature ($T > T_g$)[68] because the relaxations slightly increase the motions of macromolecular segments. The irreversible exothermic peak situated above T_g could be attributed to reactions within the lignin network, enhanced by a higher molecular mobility. As seen in Fig. 2, no significant exothermic variation is observed at $T > T_g$ for the $\Phi_{non\text{-}rev}$ curve measured during the second run. This indicates that the irreversible reactions have taken place during the thermal annealing at 135 °C. If the lignin sample is annealed at a lower temperature (*i.e.* 110 °C), an exothermic peak is detected on the $\Phi_{non\text{-}rev}$ curve (not presented here) and confirms that this phenomenon occurs within the 100–150 °C temperature interval.

In order to understand the effects of these reactions on the lignin chemical structure, IR spectra have been performed both on a water-sorbed lignin and on a lignin annealed at 135 °C (same conditions as in DSC experiments). The peak positions and assignments of the major IR bands are summarized in Table 2. As suggested by Faix[69] the absorbances have been normalized to 1 at 1516 cm^{-1}, the major absorbance peak of the aromatic skeletal vibration. The difference in absorbance can be related to small variation within chemical structure of the annealed lignin. The spectrum presented in Fig. 3 reflects structural changes occurring in the 4000–800 cm^{-1} region. This spectrum has been calculated as difference spectra between annealed and water-sorbed lignin samples. According to Table 2 and Fig. 3, the absorbance associated to O–H stretching at 3424 cm^{-1} decrease in annealed lignin as a consequence of water vaporization during the thermal treatment. The band at 1650 cm^{-1} has been assigned to H–O–H angle vibration[70] and the one at 1430 cm^{-1} to adsorption of water to carboxylic groups.[71] Then, the negative peaks found at 1650 cm^{-1} and 1428 cm^{-1} confirm the water desorption of annealed lignin. During the annealing cycle at $T > T_g$ morphological changes attributed to dehydration will induce a complete redistribution of the secondary bonds (*i.e.* hydrogen, Van der Waals bonds) in the lignin. However, the positive peak at 1214 cm^{-1} (Fig. 3) indicates that new primary bonds are also created in annealed lignin. This could be attributed to formation of aryl ether type linkages between two phenylpropane units. The β-O-4 or 4-O-5 linkages are two of the most abundant inter-unit linkages present in isolated lignins.[72] Formation of such linkages through condensation reactions during the thermal annealing at 135 °C is confirmed by a slight decrease (*i.e.* negative peak) of phenolic OH band at 1370 cm^{-1} and by an increase

Table 2 Summary of IR bands for water-sorbed and annealed (to 135 °C) AL lignin. The absorbances were normalized to 1 at 1516 cm^{-1} (absorbance peak corresponding to aromatic skeletal vibration)

Peak/cm^{-1}	Absorbance water-sorbed lignin	Absorbance annealed lignin (to 135 °C)	Assignment
3424	0.60	0.46	O–H stretching
2936	0.33	0.28	C–H stretching
1696	0.32	0.28	C═O stretching (unconjugated)
1516	1	1	Aromatic C═C vibration
1460	0.85	0.83	C–H deformation (methyl and methylene)
1425	0.49	0.45	C–H in plane with aromatic ring, vibration of carboxylic groups
1370	0.31	0.28	Phenolic OH
1328	0.57	0.54	C–O in syringyl unit
1272	0.49	0.47	C–O in guaiacyl unit
1216	1.14	1.21	C–C + C–O stretching
1152	0.31	0.30	Aromatic C–H in plane deformation (guaiacyl)
1116	1.53	1.53	Aromatic C–H in plane deformation (syringyl)
1096	0.48	0.50	C–O deformation in aliphatic ether and secondary alcohols

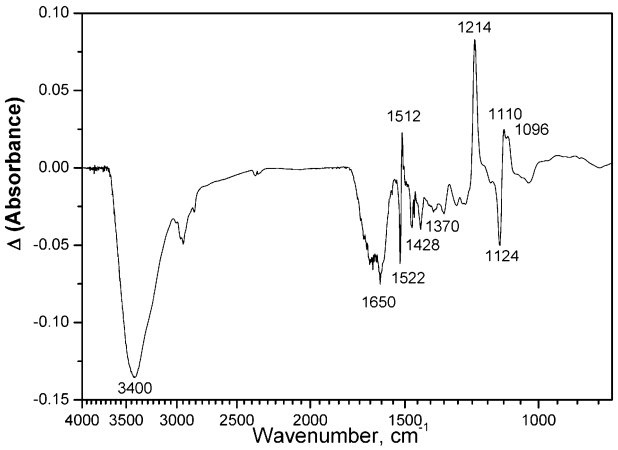

Fig. 3 Difference of IR spectra, delta (Absorbance) = Absorbance-(annealed) − Absorbance(water-sorbed lignin), in the region of 4000–800 cm^{-1}.

(*i.e.* positive peak) of C–O deformation in aliphatic ethers at 1096 cm^{-1}. As seen in Fig. 3, the splitting of the 1516 cm^{-1} band into a negative peak at 1522 cm^{-1} and a positive one at 1512 cm^{-1} is due to the shift of this band related to aromatic C═C vibrations. Moreover, the splitting of the 1116 cm^{-1} band into negative (1124 cm^{-1}) and positive peaks (1110 cm^{-1}) indicates that C–H deformations of syringyl aromatic unit are also red shifted. These slight shifts to lower wavenumbers indicate that aromatic substituents are better electron donors in annealed lignin. Such observations confirm the formation of new ether linkages during the thermal treatment at 135 °C.

According to the IR results, the three dimensional network of annealed lignin is interconnected differently compared to water-sorbed lignin due to formation of new primary as well as secondary bonds. These latter facts explain why the T_g value measured at the second run (Table 1) is shifted to higher temperature (+3 °C). Moreover, these inter-unit branchings lead to a slight increase of lignin chain connections dispersity. This fact can be directly correlated with ΔT_{set} variations observed between first and second run (Table 1). Due to the higher chain connection dispersities in annealed lignin, the relaxation times associated to this transition will have a broader distribution.

Then, the complete relaxation that corresponds to cooperatively rearranging region of the different segments occurs on a longer time scale (*i.e.* on a longer temperature interval in non isothermal mode). It is noteworthy to make a comparison between the effect of desorption and of the branching reactions on the value of the Φ_{rev} curves in the glassy state (Fig. 2). Indeed, if desorption induces a decrease of heat capacity, the branching reactions above T_g (between 100 °C and 150 °C) lead to a stiffening of the annealed sample associated with a non-reversible increase of heat capacity. Therefore, in the glassy state, it appears that the decrease due to dehydration is approximately compensated by the increase due to branching reactions. Finally, for $T > 160$ °C, the $\Phi_{non\text{-}rev}$ curves (Fig. 2) present an exothermic variation that could correspond to the onset of thermal-decomposition and/or further branching reactions at higher temperature.

To confirm the above-mentioned statements made on the irreversible phenomena, additional investigations were conducted. Vaporization, chemical reactions, or thermal-degradation can also be highlighted by thermogravimetric analysis (TGA) because they are accompanied by a weight loss. As seen in Fig. 4, a good correlation is observed during the first run between the thermogravimetric data (TGA) and the $\Phi_{\text{non-rev}}$ signal. From 25 °C to 100 °C, a weight loss of (2.6 ± 0.1)% is obtained from TGA data and corresponds to the lignin water content. This value is in perfect agreement with the precedent values (~2.8 and 2.9%) found from multifrequency DSC experiments. From 100 °C to 160 °C, the TGA curve presents a weight loss of (1.16 ± 0.03)% that could be attributed to condensations reactions or vaporization of bounded water (*i.e.* water that does not freeze at cooling). Compared to unbounded water (*i.e.* water that freeze at cooling), the vaporization of bounded water in natural polymers occurs at higher temperature.[73] According to Fig. 4, an exothermic peak is observed between 100 °C and 160 °C on the $\Phi_{\text{non-rev}}$ curve, instead of an endothermic vaporization peak. This indicates that the weight loss in this temperature domain does not correspond to vaporization of bounded water but is rather associated to exothermic reaction such as the condensations postulated above. Such weight loss could be explained by condensation reactions between phenolic rings. For $T >$ 160 °C, the TGA curve (Fig. 4) presents a variation that corresponds to the onset of thermal-degradations, in good agreement with the exothermic variation found on the $\Phi_{\text{non-rev}}$ curve in the same temperature interval. Similar onset values of thermal degradation were reported by previous studies made on various organosolv lignins.[74,75] For these isolated lignins, overall degradation has a very complex behaviour, involving several scenarios of inter-unit cleavage. To better understand this, Britt *et al.*[76,77] have used model lignin compounds to provide mechanistic insight of the main pathways involved in lignin degradation.

Additional rheometric measurements were performed both at first and second run (*i.e.* after an annealing cycle to 135 °C) to highlight the viscoelastic behaviour of lignin and to make correlations with the precedent observations. Fig. 5 represents the evolution of apparent storage (G') and loss modulii (G'', in the inset graph of Fig. 5) throughout the glass transition. Both G' and G'' drop to lower values for 110 °C < T < 175 °C, indicating a softening of the lignin matrix. The dynamic mechanical transition between the glassy and rubbery state (usually named T_α) can be estimated at the maximum of the G'' curve. This point corresponds to the maximal energy dissipated by the glass-forming liquid into cooperative motions of chain segments.[78] According to Fig. 5 (insert), $T_{\alpha(1\text{st run})}$ ~ (113 ± 2) °C whereas $T_{\alpha(2\text{nd run})}$ ~ (130 ± 3) °C. The variation of the viscoelastic response between first and second run are explained by morphological changes due to the thermal annealing. The major differences are, on one hand, the shift of $T_{\alpha(2\text{nd run})}$ to higher temperature and on the other hand, the increase of $G'_{(1\text{st run})}$ at the beginning of the relaxation process. The same measurement conducted on vacuum dried lignin (not shown on Fig. 5) presents the same rheological behaviour than the first run experiment. Thus, the differences between first and second run are not simply explained by dehydration. When measured at the first run, G' slightly increases between 80 °C and 110 °C indicating that the material become stiffer. At the beginning of the relaxation process, the decrease of G' presents a lower slope between 110 °C and 135 °C. Such observations are corroborating the precedent IR results and suggest that new inter-unit linkages are created when lignin reaches sufficient internal molecular mobility. As these inter-chain branchings improve the rigidity of lignin, they are associated with an increase of G', that partly compensate the decrease due to the relaxation process. When measured at the second run (Fig. 5), this trend is not observed, and the elastic modulus remains approximately constant before the softening. It indicates that branching reactions have occurred during the annealing cycle at 135 °C, in good agreement with above mentioned results. Moreover, the shift of $T_{\alpha(2\text{nd run})}$ to higher temperature as well as the slight increased $G'_{(2\text{nd run})}$ values in the glassy state

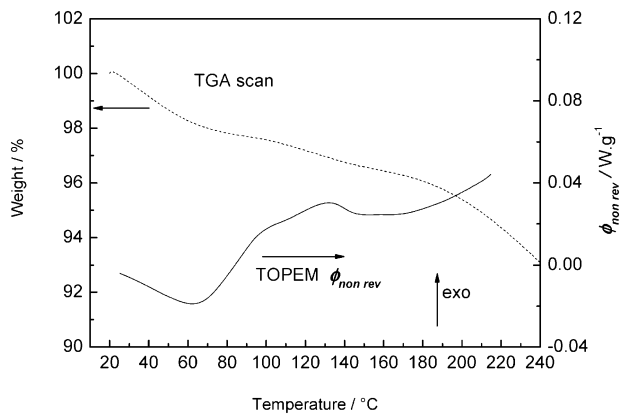

Fig. 4 Variation of mass *vs.* temperature measured by TGA on water-sorbed AL lignin at 1 K min^{-1} (dashed line) and non-reversing ($\Phi_{\text{non-rev}}$) heat flow curve (solid line) obtained from the multifrequency DSC measurements during the first run in open crucibles.

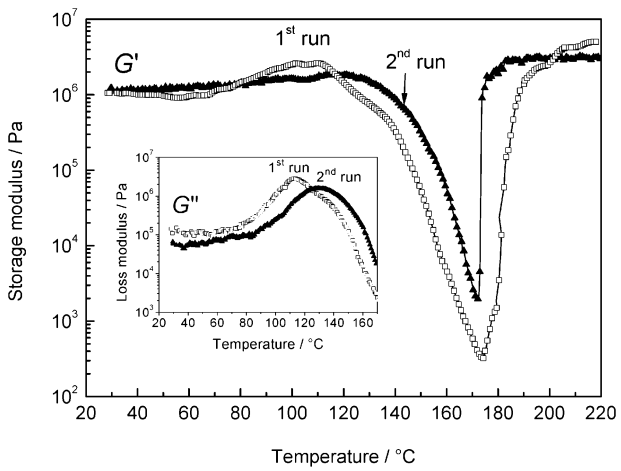

Fig. 5 Evolution of the apparent storage modulus with temperature obtained from rheometric measurements at a dynamic frequency of 1 Hz. The open squares correspond to the first heating run and the solid triangles to the second heating run after an annealing cycle to 135 °C. The inset Figure shows the evolution of the apparent loss modulus with temperature at the same rheometric parameters.

confirm that the annealed lignin has a higher degree of inter-unit linkages.

Finally, at the end of the relaxation process, a rubbery plateau is not observed as in the case of synthetic polymers. Above 175 °C, both $G'_{(1st\ run)}$ and $G'_{(2nd\ run)}$ first re-increase rapidly and then reach constant values. In this temperature region, thermal degradation and/or further branching reactions occur that are associated with a stiffening of the sample.

In the case of amorphous polymers, it is common to erase their thermal history in order to compare thermal behaviour of two samples heated from the same thermodynamic state. However, according to all the above mentioned results, when lignin is annealed at $T > T_g$ its structure is slightly modified at the microscopic scale and thus such a procedure is not applicable to the study of lignin. Thus, the use of modulated DSC (TOPEM® or TMDSC) techniques gives the opportunity to solve this analytical problem.

Plasticizing effect of water (sealed crucible experiments)

When a plasticizer is added to a classical polymer, the free volume and chain spacing increase substantially. Consequently, the glass transition is shifted to a lower temperature. As in the case of many biopolymers, the structural cohesion in lignin is insured by hydrogen bondings between the polar groups.[30] During the glass transition process, the breakage of these hydrogen bonds allows rotational or translational motions of the chain segments to take place. The plasticizing effect of water in lignin matrix is not explained by an increase of free volume but rather because water sorbs on specific polar sites and then, the nature the inter-molecular hydrogen linkages is modified.[36]

To evaluate the influence of sorbed water on T_g, experiments have been conducted in high pressure stainless steel sealed crucibles. In such devices, water cannot vaporize and remains in equilibrium between sorbed and vapour phase during the heating. The Φ_{rev} and $\Phi_{non\text{-}rev}$ curves corresponding to TOPEM® experiments in sealed crucibles are presented in Fig. 6. Here again, measurements at first and second run have been considered. As illustrated on the Φ_{rev} curves (Fig. 6), the T_g of wet AL lignin is shifted to a lower temperature (a difference of about ~30 °C) compared to the dried lignin (see Fig. 2, second run). These results highlight the plasticizing role of sorbed water and are in quite good agreement with previous DSC experiments made in hermetic conditions by Hatakeyama *et al.*[28] and Bouajila *et al.*[35] for different water contents. These authors both observed a significant decrease of T_g for a small amount of water. This decrease levels off for a certain water content that depends on lignin hydrophylicity and the saturation of specific sites. However, when measured at the first run, the Φ_{rev} curve seems to highlight two sigmoidal baseline deviations. These variations can be associated to distinct relaxation processes that have been called T_{g1} and T_{g2}, respectively in Fig. 6. The first transition (T_{g1}) is predominant and occurs at a lower temperature than the glass transition of dried lignin. This transition could be associated to the relaxation phenomena of lignin segments that are plasticized by water. On the other hand, a smaller transition (T_{g2}) that is observed at ~93 °C (*i.e.* in the same temperature

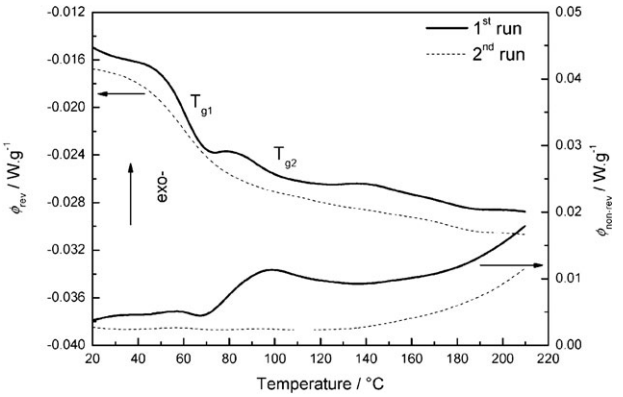

Fig. 6 Reversing (Φ_{rev}) and non-reversing ($\Phi_{non\text{-}rev}$) heat flow derived from total heat flow response to stochastic temperature pulses obtained during the heating of water-sorbed AL in sealed crucibles. The measurements were recorded during the first scan (solid line) and during the second scan (dash line) after an annealing cycle to 135 °C.

range of the dried lignin, see Table 1), could be associated to relaxation of unsorbed lignin sites. It would indicate that in wet lignin, the sorption of water on specific sites is not completely homogenous and certain parts of the sample are not water-sorbed. If we consider that ΔC_p observed for the different transitions is proportional to the amount of different systems (*i.e.* sorbed and unsorbed) the ratio $\Delta C_p(T_{g2})/[\Delta C_p(T_{g1}) + \Delta C_p(T_{g2})]$ gives the percentage of unsorbed sites in wet AL lignin. From this expression it is found that approximately 25% of the sites are unsorbed. After the annealing cycle to 135 °C (second run on Fig. 6), the Φ_{rev} curve exhibits only one single transition ($T_{mid(2nd\ run)} \sim 60$ °C) indicating that the molecular relaxation relative to the unsorbed lignin sites have disappeared. During the thermal treatment, the water has been homogenously redistributed between the different specific sites of sorption. Indeed, at $T > T_g$ the molecular motions and inter-chains spacings are more important. Then, diffusion of small molecules (such as water) into the lignin matrix is enhanced.

If we consider non-reversible thermal events, as seen in Fig. 6, the $\Phi_{non\text{-}rev}$ curve measured at the first run exhibits an exothermic peak ranging from 70 °C to 140 °C. Integration of this peak gives a total heat of ~(13 ± 2) J g^{-1} in good agreement with the precedent value of ~(13 ± 3) J g^{-1} measured in open crucible. The $\Phi_{non\text{-}rev}$ curve obtained after the annealing cycle at 135 °C does not show any residual heat released. These results are correlated with the precedent observations and confirm the hypothesis of inter-unit branching reactions for $T > T_g$. Compared to experiments conducted in open crucibles, the branching stage occurs at lower temperature (70–140 °C). It indicates that these reactions do not initiate at a given temperature but rather when chain mobility reaches a certain level. As soon as the lignin devitrifies, the inter-molecular hydrogen bonds are completely broken. The lignin segments have sufficient degrees of liberty that allow condensation reactions to take place.

For $T > 140$ °C, the $\Phi_{non\text{-}rev}$ curves present an increase in heat flux corresponding to the degradation reactions. Compared to measurements on dried lignin, the degradation phenomena starts at lower temperature (difference about −20 °C).

This support the assessment that sorbed water significantly increases the molecular mobility that is accompanied by a decrease in thermal stability of lignin. Such correlations between molecular mobility and degradation kinetics have been recently reported for PS nanoclay composites.[41]

Kinetics of lignin glass transition and size of cooperatively rearranging region

Recent studies[39–42] have investigated the dynamic of the glass transition by applying the DSC in multifrequency mode. This technique gives the glass transition at different frequencies in one single experiment. Thus, experimental errors due to series of several runs (with different samples) are avoided.

Complex heat capacity curves at varying frequency, $C^*_{p(f)}$, were evaluated from the C_{p0} curves after selection of T_g interval limits and adjustment of asymptotes corresponding to glassy and liquid-like region. For the experiments conducted using open crucibles, a series of frequencies (f) of 4, 8, 16, 24 and 32 mHz have been selected. In sealed crucibles, the τ lag is significantly higher and consequently, lower frequencies have been selected of 1.28, 1.92, 2.56 and 3.20 mHz. An example of $C^*_{p(f)}$ curves obtained at different frequencies (f) is given in Fig. 7. With increasing f, the $C^*_{p(f)}$ curves are shifted to higher temperature. It means that this transition is frequency dependent and can be associated to a cooperatively α-relaxation. Then, the corresponding apparent activation energy (E) of the glass transition can be determined from eqn (4):

$$E = -R\left(\frac{\mathrm{d}\ln f}{\mathrm{d}\,T_g^{-1}}\right) \qquad (4)$$

The mid-point temperature (T_{mid}), determined on each $C^*_{p(f)}$ curve, represents a good estimation of T_g. If we consider an Arrhenius dependence of relaxation times over the narrow interval of temperature, the slope of ln(f) *vs.* reciprocal T_{mid} yields an apparent activation energy of the lignin glass transition.

Fig. 8 shows the Arrhenius plots corresponding to the experiments in open and sealed crucibles respectively. Only second run experiments have been considered in order to avoid interaction of other thermal events (typically dehydration or branching reactions). The value of E, obtained on dehydrated lignin (*i.e.* open crucible experiment), is approximately $\sim 265 \pm 25$ kJ mol^{-1}. This value compares well with the values of 252 and 274 kJ mol^{-1} obtained in a previous multifrequency DMA analysis of *in situ* lignin glass transition.[58]

According to Fig. 8, the apparent activation energy of the lignin cooperatively α-process significantly decreases in presence of sorbed water ($E \sim 140 \pm 8$ kJ mol^{-1}). A difference of about 120 kJ mol^{-1} is found between the two systems. If we consider that hydrogen bonds strongly influence the time scales of the lignin relaxation process, then such differences of E between dehydrated and water-sorbed lignin could be correlated with these interaction strengths. It would indicate that during the glass transition phenomenon, the lignin–water hydrogen bonds are more easily broken than lignin–lignin hydrogen bonds. Consequently, the molecular motions would encounter a lower energetic barrier to take place.

The application on the Donth's equation (see eqn (1)) to the C_{p0} curves allows the V_{crr} of both sorbed and dehydrated lignin to be calculated without any microscopic model. The inset graph in Fig. 7 shows the Gaussian fit for the $C''_{p(4mHz)}$ curve (imaginary part of the complex heat capacity) used to estimate the δT value (see eqn (3)). The V_{crr} value calculated for the dehydrated lignin is $V_{crr(dehydrated)} \sim 34$ nm^3. This value is relatively high, compared to synthetic linear thermoplastic polymers, where V_{crr} varies between 0.5 and 32 nm^3.[67] Moreover the size of cooperatively rearranging region for water-sorbed lignin is $V_{crr(water\text{-}sorbed)} \sim 9$ nm^3, much smaller than for the dehydrated lignin. Such difference between the two systems outlines differences in terms of dynamic heterogeneity and is consistent with the above mentioned variation of E that shows a decrease of the energy barrier of molecular motions between dehydrated and water-sorbed lignin.

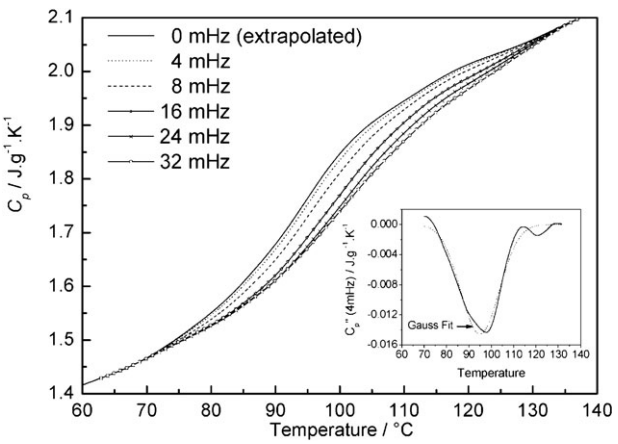

Fig. 7 "Quasi-static" heat capacity (C_{p0}) curve and the corresponding multifrequency evaluation of complex heat capacity ($C^*_{p(\omega)}$) obtained during the glass transition of water-sorbed AL lignin at the second run in open crucibles. Each frequency (in mHz) is indicated in the legend. The inset Figure shows the evolution of $C''_{p\ (4mHz)}$ and its corresponding Gaussian fit.

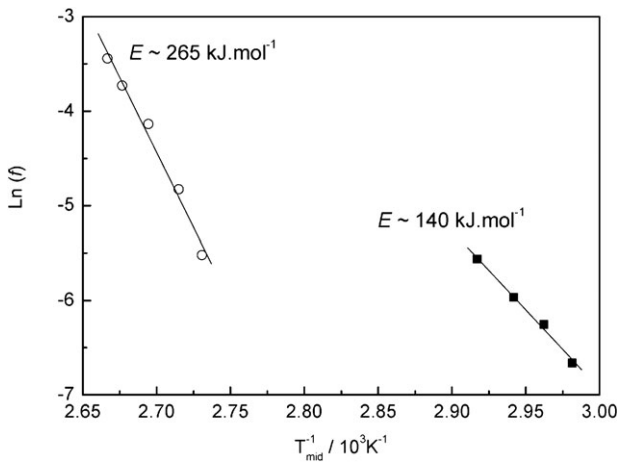

Fig. 8 Dependence of the logarithm of frequency on the reciprocal of the mid-point temperature for multifrequency DSC experiments in open crucibles (open circles) and sealed crucibles (solid squares). The linear regression corresponding to each set of data is represented by a line. The number indicated on each line corresponds to the apparent activation energy of glass transition.

In the Donth's approach, the V_{crr} represents a subsystem of a fluctuating density pattern. Recently, Beiner[79] has explained the folding process in proteins by spatial differences in the fluctuation dynamics. In the present case, the higher V_{crr} found for the dehydrated lignin indicates that probabilities of fluctuations are reduced compared to water-sorbed subsystems. This difference of segmental fluctuations can be correlated with specific interactions between lignin chains. When water is sorbed on polar sites, these interactions are significantly reduced and it leads to more mobile segments. Consequently, the conformational changes occur on shorter relaxation time and it is reflected in the decreasing volume of the cooperatively rearranging region.

The number of monomeric units (N) in one cooperatively rearranging region can be determined as follows:

$$N = V_{crr}\rho N_A/M_0 \quad (5)$$

Where ρ is the density, N_A the Avogadro number and M_0 the molecular weight of the monomeric unit. A previous proton NMR study made on Alcell lignin indicates a high percentage of phenolic groups[60] with a majority of syringyl units.[64] The predominance of syringyl over guaiacyl units is presently confirmed by IR measurements. As shown in Table 2, the relative absorbance for aromatic C–H deformation bands between guaiacyl ($A \sim 0.31$ at 1152 cm^{-1}) and syringyl ($A \sim 1.53$ at 1116 cm^{-1}) unit lead to a syringyl ratio of ~83%. Thus, if we consider the syringyl alcohol (M_0 = 184.2 g mol^{-1}) as a "representative" monomer of this lignin, it gives $N \sim 140$ syringyl units per cooperative region of dehydrated lignin. In water-sorbed lignin, this number drops to ~36 units. According to the relatively low molecular weight of this lignin ($M_w \sim 2794$ g mol^{-1}), it confirms that a cooperatively rearranging region involves large scale interactions from different lignin chains. The dense regions are smaller in water-sorbed lignin that is associated with a higher molecular mobility.

Conclusions

The molecular mobility of polymers influences dramatically their properties such as viscoelastic behaviour, chemical reactivity as well as thermal stability. The glass transition is the witness of the molecular dynamics because during this transition, a given polymer relaxes from the non-equilibrium glassy state toward the equilibrium liquid state. The evaluation of lignin glass transition from multifrequency temperature modulated DSC experiments has revealed certain original observations that are in direct links with the level of molecular mobility. When lignin is thermally annealed above its glass transition, both dehydration and non-reversible reactions take place within the lignin matrix. In the light of the obtained results, the former phenomenon leads to redistribution of secondary bonds while the latter could be explained by formation of new ether type linkages between phenylpropane units, but more complete NMR studies will be needed to confirm this hypothesis. These inter-unit branchings are associated with a slight stiffening of the annealed matrix. For water-sorbed lignin, the annealing cycle to $T > T_g$ under hermetic conditions enhances diffusion of water and allows occupation of unsorbed sites. Moreover, the higher molecular mobility in water-sorbed systems lowers T_g as well as the onset of thermal-degradations. If lignin is processed above its glass transition, inter-units linkages or thermal-degradation occur. It implies microstructural changes that are associated with an additional increase of viscosity at macroscopic scale.

Moreover, this paper demonstrates for the first time that the so-called thermal softening of isolated lignin is frequency dependant and thus can be associated to a cooperatively α-process. These results are consistent with previous literature reports that highlight the role of *in situ* lignin in the dynamics relaxation of wood. The relaxation kinetic study has shown that the molecular dynamic of isolated lignin is highly influenced by presence of sorbed water that significantly decreases the activation barrier of the relaxation process. In water-sorbed lignin, the size of cooperatively rearranging region is significantly reduced suggesting that spatial configurations are less restricted.

Acknowledgements

The authors would like to acknowledge all the partners of the ECOBINDERS project (www.ecobinders.net) and the European Commission for financial support (ECOBINDERS FP6-2003-NMP-SME-3 project). The authors acknowledge especially Richard Gosselink (University of Wageningen), Dr Pierre Bono (Granit RD) and Dr Alfred Abaecherli (ILI) for discussions about Alcell lignin. Thanks are also due to Mettler-Toledo Inc. for donating the multifrequency temperature modulated DSC (TOPEM®).

References

1 S. S. Kelley, T. G. Rials and W. G. Glasser, *J. Mater. Sci.*, 1987, **22**(2), 617–624.
2 R. Garcia, M. C. Triboulot, A. Merlin and X. Deglise, *Wood Sci. Technol.*, 2000, **34**(2), 99–107.
3 A. M. Olsson and L. Salmen, *ACS Symp. Ser.*, 1992, **489**, 133–143.
4 J. D. Gargulak and S. E. Lebo, *ACS Symp. Ser.*, 2000, **No. 742**(Lignin: Historical, Biological, and Materials Perspectives), 304–320.
5 J. H. Lora and W. G. Glasser, *J. Polym. Environ.*, 2002, **10**(1), 39–48.
6 J. S. Gratzl and C. L. Chen, *ACS Symp. Ser.*, 2000, **No. 742**(Lignin: Historical, Biological, and Materials Perspectives), 392–421.
7 C. Pouteau, S. Baumberger, B. Cathala and P. Dole, *C. R. Biol.*, 2004, **327**(9–10), 935–943.
8 C. Pouteau, P. Dole, B. Cathala, L. Averous and N. Boquillon, *Polym. Degrad. Stab.*, 2003, **81**(1), 9–18.
9 B. Kosíková, A. Revajová and V. Demianová, *Eur. Polym. J.*, 1995, **31**(10), 953–956.
10 R. Pucciariello, V. Villani, C. Bonini, M. D'Auria and T. Vetere, *Polymer*, 2004, **45**(12), 4159–4169.
11 W. de Oliveira and W. G. Glasser, *J. Wood Chem. Technol.*, 1994, **14**(1), 119–126.
12 S. Kubo and J. F. Kadla, *Macromolecules*, 2004, **37**(18), 6904–6911.
13 J. F. Kadla and S. Kubo, *Macromolecules*, 2003, **36**(20), 7803–7811.
14 A. El-Aghoury, R. Vasudeva, D. Banu, M. Elektorowicz and D. Feldman, *J. Polym. Environ.*, 2006, **14**(2), 135–147.
15 D. Banu, A. El-Aghoury and D. Feldman, *J. Appl. Polym. Sci.*, 2006, **101**(5), 2732–2748.
16 D. Feldman, D. Banu, J. Lora and S. El-Raghi, *J. Appl. Polym. Sci.*, 1996, **61**(12), 2119–2128.

17 S. S. Kelley, W. G. Glasser and T. C. Ward, *Polymer*, 1989, **30**(12), 2265–2268.
18 D. Feldman D, M. Lacasse and L. M. Beznaczuk, *Prog. Polym. Sci.*, 1986, **12**(4), 271–276.
19 Y. R. Chen and S. Sarkanen, *Cell. Chem. Technol.*, 2006, **40**(3–4), 149–163.
20 J. Wang, R. S. J. Manley and D. Feldman, *Prog. Polym. Sci.*, 1992, **17**(4), 611–646.
21 Y. Li and S. Sarkanen, *Macromolecules*, 2002, **35**(26), 9707–9715.
22 D. A. I. Goring, *Pulp Pap. Can.*, 1963, **64**(12), 517–527.
23 T. Hatakeyama and H. Hatakeyama, *Thermal Properties of Green Polymers and Biocomposites*, Kluwer Academic Publishers, Dordrecht, 2004.
24 H. Hatakeyama, J. Nakano, A. Hatano and N. Migita, *Tappi J.*, 1969, **52**(9), 1724–1728.
25 H. Hatakeyama, K. Kubota and J. Nakano, *Cell. Chem. Technol.*, 1972, **6**(5), 521–529.
26 T. Hatakeyama, K. Nakamura and H. Hatakeyama, *Polymer*, 1982, **23**(12), 1801–1804.
27 H. Yoshida, R. Morck, K. P. Kringstad and H. Hatakeyama, *Holzforschung*, 1987, **41**(3), 171–176.
28 H. Hatakeyama and T. Hatakeyama, *Thermochim. Acta*, 1998, **308**(1–2), 3–22.
29 R. J. A. Gosselink, M. H. B. Snijder, A. Kranenbarg, E. R. P. Keijsers, E. de Jong and L. L. Stigsson, *Ind. Crops Prod.*, 2004, **20**(2), 191–203.
30 S. Kubo and J. F. Kadla, *Biomacromolecules*, 2005, **6**(5), 2815–2821.
31 C. Lapierre, B. Monties, A. Vassal-Gonthier and A. Dworkin, *J. Appl. Polym. Sci.*, 1986, **32**(4), 4561–4572.
32 R. Lehnen, B. Saake and H. H. Nimz, *Holzforschung*, 2002, **56**(5), 498–506.
33 E. J. LeBoeuf and W. J. Weber, *Environ. Sci. Technol.*, 2000, **34**(17), 3632–3640.
34 Y. Uraki, S. Kubo, N. Nigo, Y. Sano and T. Sasaya, *Holzforschung*, 1995, **49**(4), 343–350.
35 J. Bouajila, P. Dole, C. Joly and A. Limare, *J. Appl. Polym. Sci.*, 2006, **102**(2), 1445–1451.
36 I. Sakata and R. Senju, *J. Appl. Polym. Sci.*, 1975, **19**(10), 2799–2810.
37 M. Reading, *Trends Polym. Sci.*, 1993, **1**(8), 248–253.
38 J. E. K. Schawe, T. Hütter, C. Heitz, I. Alig and D. Lellinger, *Thermochim. Acta*, 2006, **446**(1–2), 147–155.
39 I. Fraga, S. Montserrat and I. Hutchinson, *J. Therm. Anal. Calorim.*, 2007, **87**(1), 119–124.
40 K. Chen, K. Harris and S. Vyazovkin, *Macromol. Chem. Phys.*, 2007, **208**(23), 2525–2532.
41 K. Chen, C. A. Wilkie and S. Vyazovkin, *J. Phys. Chem. B*, 2007, **111**(44), 12685–12692.
42 S. Vyazovkin and K. Chen, *Chem. Phys. Lett.*, 2007, **448**(4–6), 203–207.
43 S. Weyer, A. Hensel, J. Korus, E. Donth and C. Schick, *Thermochim. Acta*, 1997, **304–305**, 251–255.
44 A. Hensel and C. Schick, *J. Non-Cryst. Solids*, 1998, **235–237**, 510–516.
45 J. M. Hutchinson, *Thermochim. Acta*, 1998, **324**(1–2), 165–174.
46 S. Montserrat, *J. Therm. Anal. Calorim.*, 2000, **59**(1), 289–303.
47 A. Q. Tool, *J. Am. Ceram. Soc.*, 1946, **29**(9), 240–253.
48 O. S. Narayanaswamy, *J. Am. Ceram. Soc.*, 1971, **54**(10), 491–498.
49 C. T. Moynihan, A. J. Easteal, M. A. Bolt and J. Tucker, *J. Am. Ceram. Soc.*, 1976, **59**(1–2), 12–16.
50 S. Montserrat, Y. Calventus and J. M. Hutchinson, *Polymer*, 2005, **46**(26), 12181–12189.
51 A. Hensel, J. Dobbertin, J. E. K. Schawe, A. Boller and C. Schick, *J. Therm. Anal.*, 1996, **46**(3–4), 936–954.
52 S. Weyer, M. Merzlyakov and C. Schick, *Thermochim. Acta*, 2001, **377**(1–2), 85–96.
53 S. Weyer, H. Huth and C. Schick, *Polymer*, 2005, **46**(26), 12240–12246.
54 S. Kahle, E. Hempel, M. Beiner, R. Unger, K. Schröter and E. Donth, *J. Mol. Struct.*, 1999, **479**, 149–162.
55 S. Vyazovkin, N. Sbirrazzuoli and I. Dranca, *Macromol. Rapid Commun.*, 2004, **25**(19), 1708–1713.
56 S. Vyazovkin, N. Sbirrazzuoli and I. Dranca, *Macromol. Chem. Phys.*, 2006, **207**(13), 1126–1130.
57 L. Salmén, *J. Mater. Sci.*, 1984, **19**(9), 3090–3096.
58 M. P. G. Laborie, L. Salmen and C. E. Frazier, *Holzforschung*, 2004, **58**(2), 128–133.
59 G. M. Irvine, *Wood Sci. Technol.*, 1985, **19**(2), 139–149.
60 J. H. Lora, A. W. Creamer, L. C. Wu and G. C. Goyal, in *6th International Symposium on Wood and Pulping Chemistry*, 1991, pp. 431–438.
61 W. G. Glasser, R. A. Northey and T. P. Schultz, *Lignin: Historical, Biological and Materials Perspectives, ACS symposium Series*, Oxford University Press, 742 edn., 2000.
62 R. J. A. Gosselink, A. Abächerli, H. Semke, R. Malherbe, P. Käuper, A. Nadif and J. E. G. van Dam, *Ind. Crops Prod.*, 2004, **19**(3), 271–281.
63 C. G. Boeriu, D. Bravo, R. J. A. Gosselink and J. E. G. van Dam, *Ind. Crops Prod.*, 2004, **20**(2), 205–218.
64 H. L. Hergert, G. C. Goyal and J. H. Lora, *ACS Symp. Ser.*, 2000, **No. 742**(Lignin: Historical, Biological, and Materials Perspectives), 265–277.
65 G. Adam and J. H. Gibbs, *J. Chem. Phys.*, 1965, **43**(1), 139–146.
66 E. Donth, *J. Polym. Sci., Part B: Polym. Phys.*, 1996, **34**(17), 2881–2892.
67 E. Hempel, G. Hempel, A. Hensel, C. Schick and E. Donth, *J. Phys. Chem. B*, 2000, **104**(11), 2460–2466.
68 N. Sbirrazzuoli, A. Mititelu-Mija, L. Vincent and C. Alzina, *Thermochim. Acta*, 2006, **447**(2), 167–177.
69 O. Faix, in *Fourier Transform Infrared Spectroscopy*, eds. S. Y. Lin and C. W. Dence, Methods In Lignin Chemistry, Springer-Verlag, Berlin, Heidelberg, 1992, pp. 89–103.
70 K. Haxaire, Y. Maréchal, M. Milas and M. Rinaudo, *Biopolymers*, 2003, **72**(1), 10–20.
71 A.-M. Olsson and L. Salmén, *Carbohydr. Res.*, 2004, **339**(4), 813–818.
72 W. G. Glasser, C. A. Barnett, P. C. Muller and K. V. Sarkanen, *J. Agric. Food Chem.*, 1983, **31**(5), 921–930.
73 S. Vyas, S. Pradhan, N. Pavaskar and A. Lachke, *Appl. Biochem. Biotechnol.*, 2004, **118**(1), 177–188.
74 F. Xu, J. X. Sun, R. Sun, P. Fowler and M. S. Baird, *Ind. Crops Prod.*, 2006, **23**(2), 180–193.
75 J. C. Domínguez, M. Oliet, M. V. Alonso, M. A. Gilarranz and F. Rodríguez, *Ind. Crops Prod.*, 2008, **27**(2), 150–156.
76 P. F. Britt, A. C. Buchanan, M. J. Cooney and D. R. Martineau, *J. Org. Chem.*, 2000, **65**(5), 1376–1389.
77 P. F. Britt, M. K. Kidder and A. C. Buchanan, *Energy Fuels*, 2007, **21**(6), 3102–3108.
78 T. G. Metzger, *The Rheology Handbook*, Vincentz Network, Hannover, 2nd edn, 2006.
79 M. Beiner, *Soft Matter*, 2007, **3**, 391–393.

